Label-Free In-Flow Detection of Single DNA Molecules using Glass Nanopipettes

ARTICLE *in* ANALYTICAL CHEMISTRY · DECEMBER 2013

Impact Factor: 5.64 · DOI: 10.1021/ac403391q · Source: PubMed

8 AUTHORS, INCLUDING:

Amol V Patil
Imperial College London
19 PUBLICATIONS **153** CITATIONS
SEE PROFILE

Aleksandar P Ivanov
Imperial College London
20 PUBLICATIONS **311** CITATIONS
SEE PROFILE

Qingyuan Kong
Imperial College London
1 PUBLICATION **14** CITATIONS
SEE PROFILE

analytical chemistry

Article

pubs.acs.org/ac

Label-Free In-Flow Detection of Single DNA Molecules using Glass Nanopipettes

Xiuqing Gong,[§] Amol V. Patil,[†,§] Aleksandar P. Ivanov,[†] Qingyuan Kong,[†] Thomas Gibb,[†] Fatma Dogan,[†] Andrew J. deMello,[‡] and Joshua B. Edel*[,†]

[†]Department of Chemistry, Imperial College London, South Kensington Campus, London SW7 2AZ, United Kingdom

[‡]Institute for Chemical and Bioengineering, Department of Chemistry and Applied Biosciences, ETH Zürich, 8092 Zürich, Switzerland

Supporting Information

ABSTRACT: With the view of enhancing the functionality of label-free single molecule nanopore-based detection, we have designed and developed a highly robust, mechanically stable, integrated nanopipette-microfluidic device which combines the recognized advantages of microfluidic systems and the unique properties/advantages of nanopipettes. Unlike more typical planar solid-state nanopores, which have inherent geometrical constraints, nanopipettes can be easily positioned at any point within a microfluidic channel. This is highly advantageous, especially when taking into account fluid flow properties. We show that we are able to detect and discriminate between DNA molecules of varying lengths when motivated through a microfluidic channel, upon the application of appropriate voltage bias across the nanopipette. The effects of applied voltage and volumetric flow rates have been studied to ascertain translocation event frequency and capture rate. Additionally, by exploiting the advantages associated with microfluidic systems (such as flow control and concomitant control over analyte concentration/presence), we show that the technology offers a new opportunity for single molecule detection and recognition in microfluidic devices.

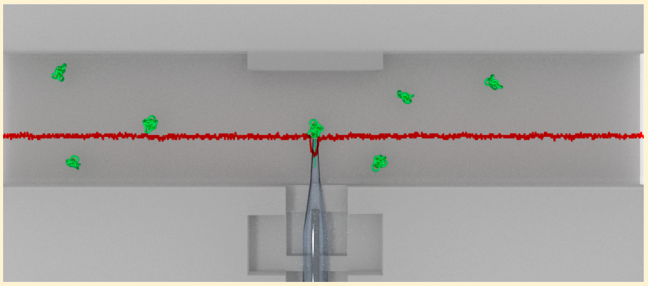

Single molecule detection (SMD), which enables the measurement of structural and chemical variance of "apparently identical" molecules, has been one of the ultimate goals in chemical analysis. This is predominantly due to the removal of ensemble averaging or "blurring" of the acquired data, resulting in an extremely valuable tool in a range of applications such as the detection of point mutations[1] and protein folding.[2,3] Although over the last 25 years, fluorescence techniques have been the most popular due to their inherent sensitivity, there is currently a drive to develop label-free approaches such as those based on micro/nanocantilevers,[4] nanowires,[5] and nanopores.[6,7] Importantly, the inherent and significant advantages of nanopore sensors have yielded many new applications which cannot readily be realized using more conventional techniques. Indeed, current technology is at a state where it is possible to differentiate between nucleosomal substructures,[8] keys pairs of RNA polymerase DNA transcription,[9] and protein discrimination using either bare[3] or aptamer-modified pores with an ionic current blockade and sensing modality.[10,11] Moreover, it is feasible to enhance the functionality of such nanopore platforms by incorporating optical detection,[12−14] single molecule force techniques,[15] or tunnelling detection.[16,17]

A solid-state nanopore is typically fabricated by drilling a nanoscale aperture (usually with sub-50 nm diameter) in a thin insulating membrane, made from low-stress silicon nitride, which separates two macroscale chambers containing electrolytic solution.[18,19] Upon application of a voltage bias across the membrane, ionic current flows through the pore, with a magnitude determined by the pore dimensions and the electrolyte concentration. When a charged biomolecule stochastically enters the pore, thus occluding the nanopore, the ionic current either increases or decreases depending upon the biomolecule size, structure, and surface charge.[7] By controlling the pore dimensions/materials,[20−22] surface properties of the pore,[23,24] electrolyte conditions,[25] and applied voltage bias, it is possible to discriminate between biomolecule types and populations. An obvious limitation of the described format (i.e., two macroscale chambers) is the implicit large volume of the analyte sample relative to the nanometer-sized capture area. As a result, only a very small subset of all molecules that are sufficiently close to the nanopore can be detected.

To truly achieve their full potential, such sensors either need to achieve more efficient transfer of analyte molecules toward the detection zone or alternatively must confine the analyte to a volume that has similar dimensions to that of the nanopore. By doing so, high-throughput analysis with high detection

Received: October 18, 2013
Accepted: December 11, 2013
Published: December 11, 2013

   dx.doi.org/10.1021/ac403391q | *Anal. Chem.* 2014, 86, 835−841

efficiency becomes possible. One solution in this regard is to use microfluidic systems to guide and deliver fluid flow to the nanopore. Added benefits of such an approach include the ease of sample change, higher analytical throughput,[26] and the ability to multiplex. At a fundamental level, the appeal of such a hybrid device is motivated by the fact that physical and chemical processes can be controlled and harnessed more easily when analytical volumes are reduced to the subnanoliter scale. However, the integration of a nanopore with a microfluidic device is a nontrivial, time-consuming task, requiring access to complex and expensive semiconductor processing technology such as clean room facilities, focused electron/ion beam instrumentation, and photolithographic tools. Accordingly, the complexity in fabrication does not necessarily outweigh the potential analytical benefits. Furthermore, typical issues in solid-state nanopore sensing such as low resistivity and high dielectric losses (that cause increased electrical noise) generally leads to a reduction in the utility of hybrid devices. Moreover, a geometrically planar solid-state nanopore would typically act as one of the microfluidic channel walls. Assuming a laminar Poiseuille flow profile, the active area of the nanopore will be within the zero flow (no-slip) regime, resulting in flow within the channel having limited benefit. All the above issues have resulted in relatively few literature reports that describe the successful integration of nanopores with microfluidics.[27,28]

A viable alternative that can address all of the above limitations are quartz/borosilicate nanopipettes. They are inexpensive to fabricate, quick to make (<10 s), electrically and chemically stable, exhibit low noise, and can easily be made with pore radii ranging from 15 to several hundred nanometers.[29,30] In contrast to solid-state nanopores, the cylindrical nanopipette geometry can be placed at any location (including the geometric center) within a microfluidic channel, thus enabling high analyte capture rates, while minimizing sample usage. In simple terms, a nanopipette, with its large aspect ratio, provides a direct and facile way of integrating nanofluidic and microfluidic structures, thus enabling new features and functions on the nanoscale to be coupled with microfluidic components.

The vast majority of the nanopipette literature has focused on using such platforms as electrochemical sensors, cell injectors, or for use in DNA/protein deposition.[31−34] Importantly, there is also emerging evidence that nanopipettes can be used for label-free single molecule detection and recognition when coupled with pulse-resistive methods.[35−39] In the current manuscript, we present a facile method for integrating a nanopipette with a microfluidic chip that address most of the existing limitations of solid-state nanopore and associated difficulties with microfluidic integration, for biomolecular detection and characterization of such a nanopipette-microfluidic device. To our knowledge, this is the first report of successful continuous-flow detection of single DNA molecules by a composite nanopipette/microfluidic device.

EXPERIMENTAL SECTION

The fabricated hybrid nanopipette-microfluidic platform consists of two components, a quartz nanopipette and a polydimethylsiloxane (PDMS)-based microfluidic device. Nanopipettes were pulled on a laser pipet puller (P2000, Sutter Instruments) using quartz capillaries with filament (i.d., 0.5 mm; o.d., 1 mm; length, 7.5 cm; Sutter Instruments). Pipette pulling involves a two-step program: (1) HEAT: 575; FIL: 3; VEL: 35; DEL: 145; PUL: 75, followed by (2) HEAT: 900; FIL: 2; VEL: 15; DEL: 128; PUL: 200. The first cycle pulls a 1.5 mm taper length out of the capillary, while the second cycle pulls the capillary further till breaking. It should be noted that the pulling program is instrument-specific, and there is variation between P2000 pullers.

Microfluidic devices were fabricated using standard soft lithographic methods (see Figure SI-1 of the Supporting Information). The PDMS precursor mixture was poured over a lithographically fabricated silicon master and cured on a hot plate at 60 °C for 120 min. The cured PDMS substrate, a nanopipette, and a 160 μm thick glass coverslide (VWR International Ltd., Leicestershire, U.K.) were cleaned using a plasma cleaner (SPI Plasma Prep, West Chester, PA). The nanopipette was manually positioned in the side channel, with the glass slide sealing off the microfluidic device. Finally, semicured PDMS was used to seal the gap between the nanopipette and PDMS chip (see Figure SI-2 of the Supporting Information).

DNA translocation studies were carried out using 48.5 kbp λ-DNA (New England Biolabs Inc., catalogue no: N3011S) as well as 5 kbp and 10 kbp λ-DNA fragments. All samples were diluted to a concentration of 1 nM in 1 M KCl, 10 mM Tris, and 1 mM EDTA. All solutions were filtered using a 0.2 μm lure lock syringe filter (Millex syringe filters, EMD Millipore) to remove large particulates.

To allow biomolecule introduction without disturbing flow within the microfluidic channel, a sample injector valve (7725i Rheodyne, Sigma Aldrich, Gillingham, U.K.) equipped with a 100 μL sample loop was utilized. The valve inlet was connected to a 1 mL glass Hamilton syringe (Hamilton Company) mounted on syringe pump (PHD 2000, Harvard Apparatus, U.K.), using electrically shielded soft tubing, with the valve outlet connected to the PDMS microfluidic device inlet.

Ionic current was measured by applying a voltage bias across freshly chloridized Ag/AgCl electrodes (0.125 mm diameter, GoodFellow U.K.); one electrode was placed inside the nanopipette and the other was placed in the main channel exit reservoir. The entire setup was placed in a Faraday cage with a dedicated low noise ground connection and mounted on a vibration isolation table. The current signal was measured with an Axopatch 200b low noise current amplifier (Molecular Devices) in "voltage clamp" mode. Data were low-pass filtered at 5 kHz using the built-in 8 pole Bessel filter. The output signal was sent to a Digidata 1440A data-acquisition module (Molecular Devices), digitized at 50 kHz and recorded using pClamp 10.2 software (Molecular Devices). The "open pore" current was recorded prior to insertion of the double-stranded DNA in the microfluidic device. Data analysis was carried out using a combination of Clampfit 10.2 and a home-written MatLab analysis routine.

For each DNA sample, between 250 and 750 translocation events were recorded for statistical analysis. The baseline current was calculated using a moving window average for every 5 data points. Only events with a current amplitude higher than 6 standard deviations from the baseline current were considered.

RESULTS AND DISCUSSION

The resulting hybrid nanopipette-microfluidic device has a high aspect ratio and contains a tapered quartz tip that terminates in a nanometer size pore. Due to fabrication limitations, the pore diameter is typically inversely proportional to the taper length. Moreover, since the surface of the quartz capillary is negatively

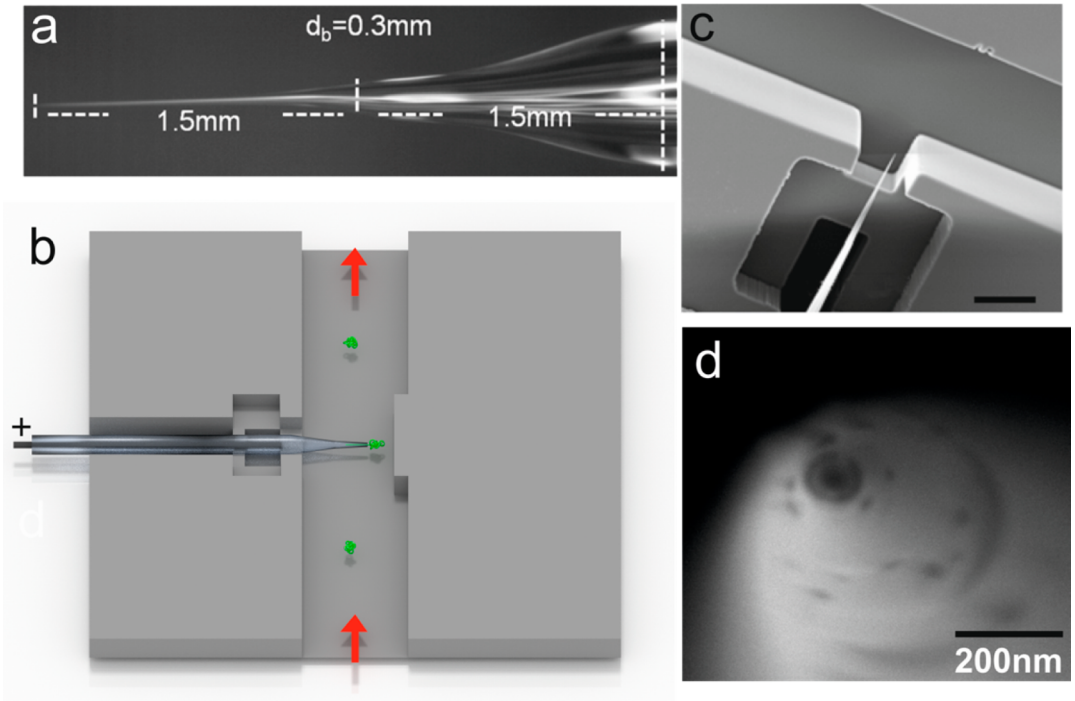

Figure 1. (a) Optical micrograph of the nanopipette showing the dimensions of the tip, shank, and shoulder. (b) Schematic diagram illustrating the nanopipette integrated microfluidic device. The red arrow indicates the direction of flow. (c) SEM image of the nanopipette embedded within the microfluidic channel (scale bar: 50 μm). (d) SEM image of the tip of the nanopipette.

charged, when contained in an electrolyte above pH 6, a diffusive electric double layer is formed across the nanopipette, affecting ion transport properties induced by an applied voltage bias.[40] These effects unfortunately result in an increase in electrical noise with increasing taper length and decreasing pore radius. Hence, a custom fabrication recipe was developed to ensure a short taper length (less than 2 mm), while keeping the nanopore diameter below 50 nm (Figure 1a). The nanopipette, with a shank length of about 1.5 mm and pore diameter of 40 nm, was fabricated from a quartz capillary (Sutter Instruments), pulled using a laser pipet puller (P-2000 Laser Based Puller, Sutter Instruments). It should be mentioned that by increasing the taper length, the surface area of the nanopipette increases causing an increase in the double layer. Furthermore, a long taper requires a thinner quartz wall, thus causing a higher leakage noise due to capacitive current. While a smaller nanopipette can be used and would be expected to have a higher resistance, in our experience, the signal-to-noise ratio is not affected drastically.

The nanopipette is aligned and assembled within the center of a microfluidic channel made from PDMS. A T-type side channel was incorporated into the design to feed in the nanopipette (Figure1, panels b and c). A two-step lithographic process was used to fabricate the microfluidic channel. This was needed so that that nanopipette would rest on a "pedestal" and ensure that the inserted tip was located in the center of the channel (Figure 1c). Such an arrangement also prevents possible contamination between the pore and PDMS structure. A finite element analysis of the device shows that the pore at the very end of the nanopipette tip is exposed flow rates that depend upon the pore's position relative to the microfluidic channel wall (i.e., a nanopipette placed within 10 μm of the microfluidic channel center would see a higher flow rate than a solid-state nanopore integrated into the wall of the microfluidic channel (Figures SI-3 and SI-4 of the Supporting Information). This is due to the flow rate, tending to zero in the region of the walls of the fluidic channel.

In a typical experiment "DNA-free" (10 mM Tris-HCl, 1 mM EDTA, pH 8) buffer containing 1 M KCl was initially introduced at a flow rate of 1 μL/min to prime the microfluidic device. Ag/AgCl electrodes were placed inside the nanopipette while a counter electrode was placed downstream at the exit reservoir. By sweeping the applied voltage bias (between the nanopipette and microfluidic channel) from +500 to −500 mV, the electrical connectivity and the current−voltage properties can be mapped). The typical conductance (G) in 1 M KCl buffer is approximately 70 nS. The inner diameter of the nanopipette (d_i) can also be estimated using $d_i = 4Gl/\pi g d_b$, where l is the length of the conical area of the nanopipette (approximately 1.5 mm as shown in Figure 1), d_b is the diameter of the nanopipette before convergence (300 μm), and g is the conductance (11.2 S/m) of 1 M KCl. The estimated inner diameter of 40 nm is in good agreement with SEM images (Figure 1d) and demonstrates that there is no damage to the pore at the tip of the nanopipette during composite microfluidic-nanopipette device fabrication. To confirm fabrication reproducibility, more than seven such devices were fabricated with similar pore diameters and in all cases similar conductance values (Figure SI-5 of the Supporting Information). As anticipated, the ionic current was stable at an applied bias between 100−500 mV and flow rates ranging between 0.1−10 μL/min. For example, at 500 mV, the root-mean-square of the ionic current was found to be ∼7 pA, which compares favorably with published reports for SiN_x solid-state nanopores.[41]

To maintain a stable flow and thus minimize disruption in the ionic current, DNA was introduced via a rheodyne injection valve and transported downstream toward the nanopore. As the

dx.doi.org/10.1021/ac403391q | Anal. Chem. 2014, 86, 835−841

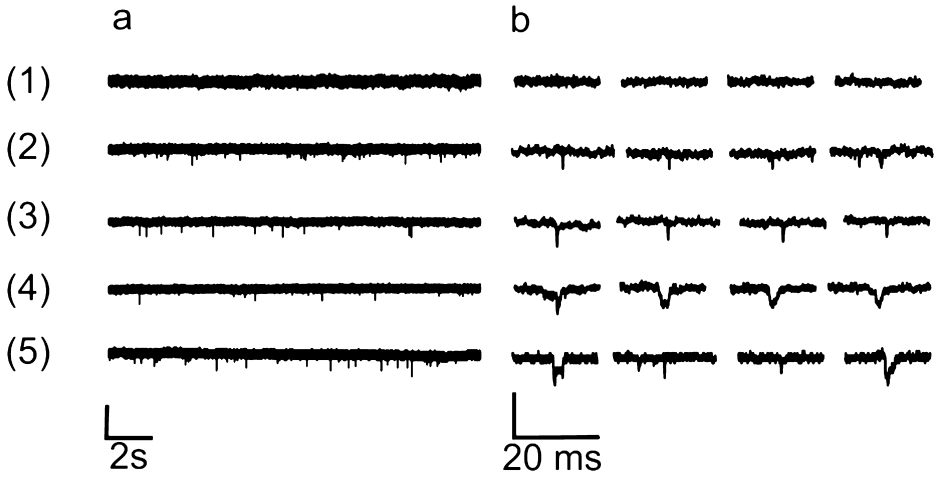

Figure 2. (a) Extract from a typical two mintute long current time trace as obtained at an applied bias of 500 mV for (1) blank buffer (2) 5 kbp (3) 10 kbp (4) 48.5 kbp (5) mixture of 5 kbp and 48.5 kbp DNA. (b) Magnified view highlighting translocation events (current scale bar: 100 pA).

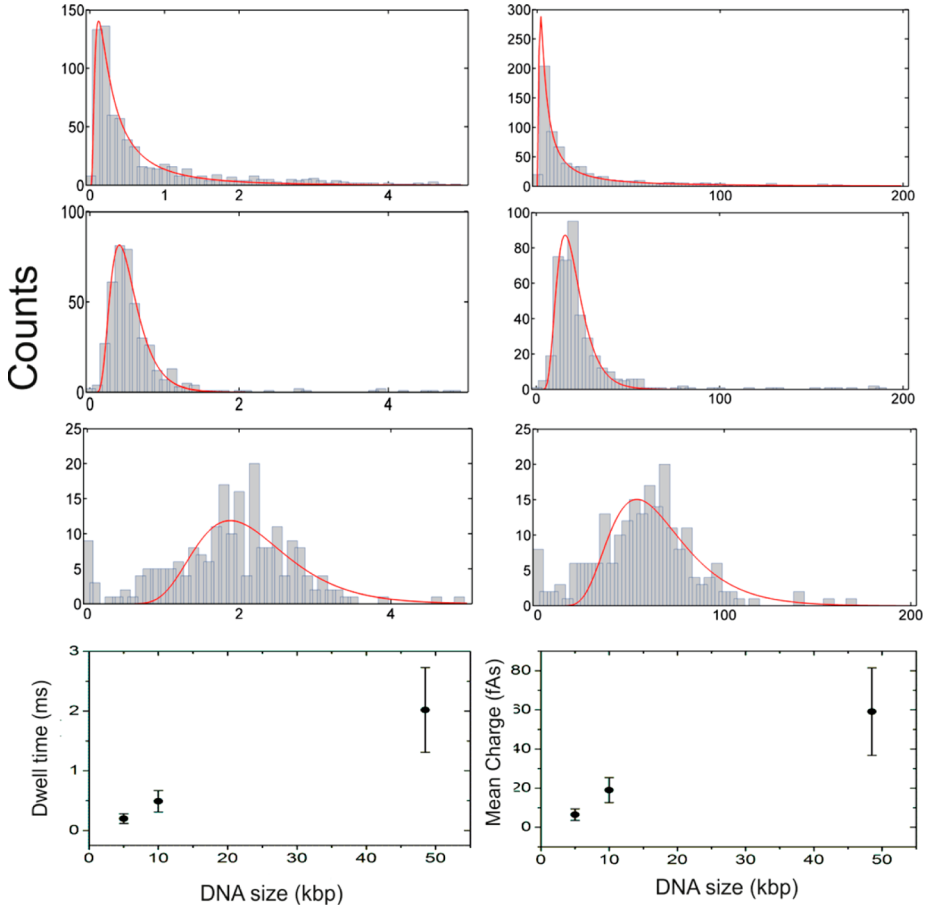

Figure 3. Translocation statistics at an applied bias of 500 mV and flow rate of 1 μL/min for 5, 10, and 48.5 kbp DNA is shown. In all cases fits to the histrograms are shown in red.

molecule threads through the nanopore, the resulting occlusion causes a momentary decrease in the ionic current as observed in the literature.[39] To demonstrate DNA detection within flow regime, a 5 kbp sample was initially injected into the microfluidic chip at a flow rate of 1 μL/min and with an applied voltage bias of 500 mV. As can be seen in Figure 2, characteristic translocation events can be clearly observed above background. After 20 min of continuous recording of the ionic current, clean DNA-free buffer was injected to flush out residual DNA molecules from the microfluidic device. Subsequently, 10 kbp and 48.5 kbp λ-DNA samples were introduced sequentially (Figure 2; 10 kbp and 48.5 kbp), each following flushing steps with DNA-free buffer.

Composite event histograms of the dwell time (τ_d), integrated current area per translocation, and the peak current for DNA lengths of 5, 10, and 48.5 kbp are shown in Figure 3. Both dwell time and integrated charge histograms scale with the molecular length and can clearly be discriminated for each

dx.doi.org/10.1021/ac403391q | Anal. Chem. 2014, 86, 835−841

DNA sample. For 5 kbp DNA, the mean τ_d was found to be 0.20 ± 0.08 ms. The mean values of dwell time and charge were calculated using recently reported first-passage probability density function (FP-PDF), $F_1(t) = (L/(4\pi Dt^3)^{1/2} e^{-(L-\nu t)^{2/4Dt}}$, where D is the diffusion constant, v the drift velocity, and L is the contour length of the DNA, unlike the Lubensky–Nelson model[42] (assumes a rigid rod structure for the DNA with no configuration entropy with absorbing boundary condition on the cis and trans side), and is based upon Schrödinger's first-passage-time theory with a single absorbing boundary condition and yields information about the drift velocity and diffusion constant of the DNA within the pore.[43] For 10 kbp and 48.5 kbp DNA, τ_d was determined to be 0.49 ± 0.18 and 2.02 ± 0.71 ms, respectively. These results are in good agreement with literature (1.56 ms for unfolded 48.5 kbp DNA using nanopipettes in bulk solution).[39] Furthermore, these observations are consistent with translocation times associated with solid-state nanopores.[44,45] For DNA molecules of 5, 10, and 48.5 kbp, the average contour lengths are 1.7, 3.4, and 16.5 μm, respectively. This results in similar translocation speeds of 8.5, 7.5, and 8.2 mm/s, which are again in good agreement with literature.[39,44−46] Additionally, the excluded charge per translocation event (measured as the integrated current area per translocation) is expected to be constant for molecules of the same size.[39] For 5, 10, and 48.5 kbp DNA, we measured a mean integrated charge of 6.48 ± 2.93, 19.02 ± 6.38, and 59.12 ± 22.34 fAs, respectively. The latter value is in excellent agreement with the 67 fAs mean integrated charge already reported for 48.5 kbp DNA.[39] Importantly, the charge histograms only provide evidence for a single population, indicating that the flushing step was efficient with no measurable contamination from previous runs.

In order to quantify device parameters, translocation events for 48.5 kbp DNA molecules were further analyzed to assess any dependence of translocation event frequency (defined as the total number of translocation events occurring per minute) on applied voltage bias and flow rate (Figure 4). Capture of DNA molecules into the nanopipette pore occurs due to a complex interplay of convection (if flow is present), diffusion down the microfluidic channel, and electrophoretic movement toward the pore (due to the applied voltage bias). No translocation events were observed until the applied bias voltage reached a value of 200 mV (an observation that is valid for all of the DNA molecules irrespective of their length) (Figure 4a), indicating the existence of an energy barrier that prevents entry of the biomolecule into the nanopipette. This behavior is in agreement with previous reports, which highlight that a minimum voltage bias is required for a DNA molecule to overcome the translocation energy barrier to enter a biological pore.[47,48]

Similar to the capture of single-stranded DNA into a lipid-embedded α-hemolysin pore, the DNA capture rate (R; defined here as directly corresponding to the translocation event frequency) is either dependent on the diffusion-limited capture rate R_{diff} or barrier-limited capture rate (R_{bar}).[25,49] In the diffusion-limited process, the capture rate limiting step is diffusion of the biomolecule to a capture hemisphere of radius r^* and given as $R_{diff} = 2\pi Dr^* = \pi d^2\mu/4l\Delta V$. Here, D is defined as the DNA coil diffusion coefficient, and μ is the electrophoretic mobility of the DNA coil, r^* is the effective capture radius (the distance from nanopore where DNA moves from purely diffusive to voltage-biased motion), d is the pore

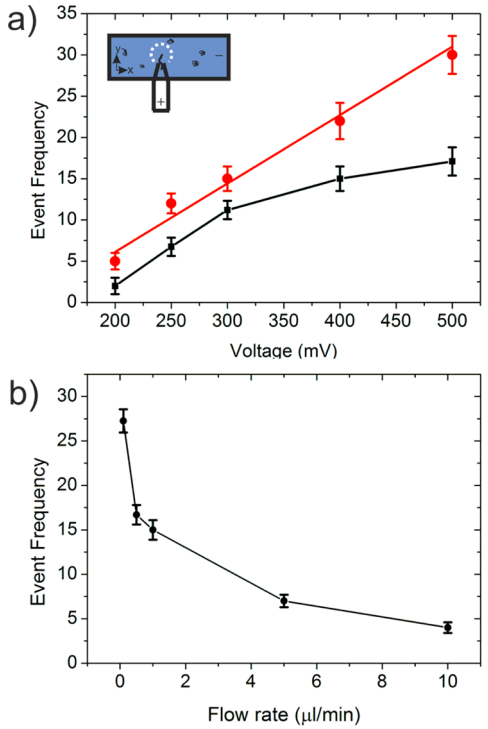

Figure 4. (a) Translocation event frequency of 48.5 kbp DNA as a function of voltage without flow (red) and with a flow rate fixed at 1 μl/min (black). (b) Translocation event frequency as a function of flow rate at a fixed bias of 500 mV.

diameter, ΔV is the applied voltage bias, and l is the pore length (Figure 4a, inset). The red curve in Figure 4a demonstrates the linear relationship between R_{diff} and applied voltage bias, yielding a slope of 0.08 V^{-1} in the absence of flow.

However, if the flow rate increased to 1 μL/min (Figure 4a, black curve), a logarithmic behavior in event frequency is observed with increasing applied voltage bias. This is markedly different from the reported exponential dependence of capture rate on applied voltage bias in the barrier-limited capture rate (R_{bar}) observed in smaller pores.[50,51] With a fixed applied bias (500 mV), as the flow rate was varied between 0.1 and 10 μL/min, the translocation event frequency showed a logarithmic decrease, as shown in Figure 4b. This behavior could be interpreted in terms of the limitations imposed by laminar flow on molecular transverse diffusion.[52] In a pressure-driven laminar flow regime within a microchannel, the width of molecular diffusion $\delta(y,z)$ in the y,z direction (with z being perpendicular to the plane of the figure) (Figure 4a, inset) obeys a power-law dependence much like the average flow rate [i.e., $\delta(y,z) \propto (DHx/U_a)^{0.5}$].[53] Here, D is the diffusion coefficient, H is the given height of the channel, x is the distance along the flow direction, and U_a is the average flow rate. Thus in other words, with a laminar flow in a direction perpendicular to the nanopipette, increasing the flow rate causes a reduction in any lateral diffusion of the DNA molecule toward the nanopore. Additionally given an applied voltage bias of 500 mV, the translocation velocity of 48.5 kbp DNA is ~8.2 mm/s, while the downstream buffer flow velocity scales from 1.48 mm/s (for 1 μL/min) to 14.8 mm/s (for 10 μL/min).

On first inspection, it might appear that the reduction in translocation event frequency with increasing flow rate nullifies the perceived advantage of microfluidic devices, namely high-throughput analysis; however, this device parameter is advanta-

dx.doi.org/10.1021/ac403391q | Anal. Chem. 2014, 86, 835−841

geous as it allows the user to rapidly introduce a particular analyte population, decelerate the flow rate, measure the translocation parameters, and then accelerate the flow rate to prepare the device for the next analyte population (without cross contamination). To assess the ability to distinguish and identify a target molecule within a complex mixture, 1 nM solutions of 5 and 48.5 kbp DNA were premixed at a 1:1 molar ratio with an applied voltage bias of 500 mV. The results of such an analysis are illustrated in the histogram and scatter plots presented in Figure 5. A "k-means" cluster analysis

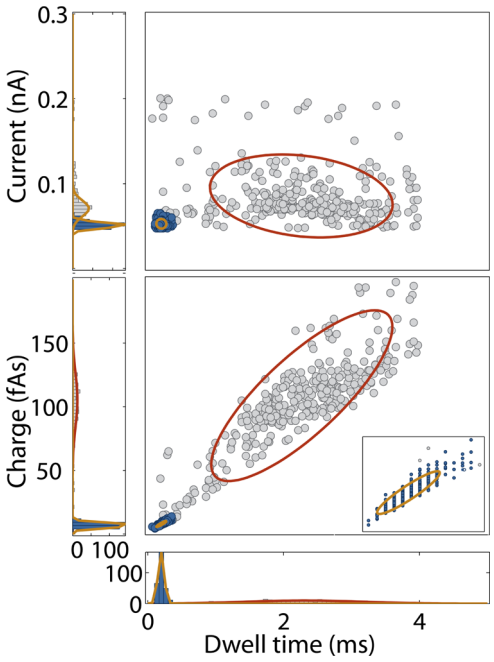

Figure 5. Translocation statistics for a 1:1 mixture of 1 nM solutions of 5 kbp and 48.5 kbp at a fixed applied bias of 500 mV and a flow rate of 1 μL/min. A k-means cluster analysis was carried out using a custom written Matlab algorithm where two characteristic populations in the current−dwell time scatter plots could be identified (5 kbp in blue and 48.5 kbp in grey). The inset shows a magnified plot of the blue cluster.

identifies two characteristic populations in the current−dwell time scatter plot (Figure 5, left). The dashed ellipses in Figure 5 outline the different populations within a 68% confidence interval. The current drop as a function of dwell time clusters as two populations with mean τ_d values of 0.21 ± 0.04 and 2.05 ± 1.58 ms. It is noted that both of these values are very similar to the mean τ_d values of 0.20 ± 0.08 ms and 2.02 ± 0.71 ms obtained in experiments with individual 5 and 48.5 kbp DNA populations. Additionally, we also calculated an integrated charge−dwell time scatter plot (Figure 5, right). Again, the scatter plot values were linearly distributed in two populations with distinct slope coefficients (each corresponding to the mean translocation peak current for the population). These results confirm the ability of nanopipette detection within a microfluidic platform to accurately discriminate DNA populations of different size in mixed solutions and in flow.

CONCLUSIONS

We have presented the first successful demonstration of incorporating nanopipettes within microfluidic channels for in-flow label-free single molecule sensing. We show that it is possible to control both flow rate and applied bias, while still maintaining single molecule capability with low noise. The aspect ratio of the nanopipette enables easy positioning of a nanoscale pore at the apex of a macroscopic body in the high flow zone of the microfluidic device.

Both under no-flow and flow conditions, expected current drops (whose magnitude and duration depend upon molecular length and structure) were observed that indicate translocation of single-analyte molecules through the nanopipette upon application of an appropriate voltage bias. Detailed characterization of the device indicates an opposing contribution of flow toward the translocation of analyte through the nanopipette (i.e., as flow rate increases, the capture frequency decreases). The total analysis time can be minimized by implementing continuous sample loading, with high flow rate flush steps between samples enabling characterization of different analytes with the same device. This is an important step in achieving true label-free single molecule detection within microfluidic devices. Furthermore, the robustness and versatility of this device has many potential applications in the detection of single DNA and protein molecules in combination with other (e.g., optical) detection systems.

ASSOCIATED CONTENT

Supporting Information

Additional information as noted in text. This material is available free of charge via the Internet at http://pubs.acs.org.

AUTHOR INFORMATION

Corresponding Author

*E-mail: joshua.edel@imperial.ac.uk.

Author Contributions

§X.G. and A.V.P. contributed equally.

Notes

The authors declare no competing financial interest.

ACKNOWLEDGMENTS

This work was supported, in part by an Engineering and Physical Sciences Research Council (EPSRC) grant and an ERC Starting Investigator grant.

REFERENCES

(1) Ingebrandt, S.; Han, Y.; Nakamura, F.; Poghossian, A.; Schoning, M. J.; Offenhausser, A. *Biosens. Bioelectron.* **2007**, *22*, 2834.
(2) Lipman, E. A.; Schuler, B.; Bakajin, O.; Eaton, W. A. *Science (New York, N.Y.)* **2003**, *301*, 1233.
(3) Japrung, D.; Dogan, J.; Freedman, K.; Nadzeyka, A.; Bauerdick, S.; Albrecht, T.; Kim, M. J.; Jemth, P.; Edel, J. B. *Anal. Chem.* **2013**, *85*, 2449.
(4) Ziegler, C. *Anal. Bioanal. Chem.* **2004**, *379*, 946.
(5) Bunimovich, Y. L.; Shin, Y. S.; Yeo, W.-S.; Amori, M.; Kwong, G.; Heath, J. R. *J. Am. Chem. Soc.* **2006**, *128*, 16323.
(6) Dekker, C. *Nat. Nano* **2007**, *2*, 209.
(7) Miles, B. N.; Ivanov, A. P.; Wilson, K. A.; Dogan, F.; Japrung, D.; Edel, J. B. *Chem. Soc. Rev.* **2013**, *42*, 15.
(8) Soni, G. V.; Dekker, C. *Nano Lett.* **2012**, *12*, 3180.
(9) Raillon, C.; Cousin, P.; Traversi, F.; Garcia-Cordero, E.; Hernandez, N.; Radenovic, A. *Nano Lett.* **2012**, *12*, 1157−1164.
(10) Cressiot, B.; Oukhaled, A.; Patriarche, G.; Pastoriza-Gallego, M.; Betton, J.-M.; Auvray, L.; Muthukumar, M.; Bacri, L.; Pelta, J. *ACS Nano* **2012**, *6*, 6236.
(11) Rotem, D.; Jayasinghe, L.; Salichou, M.; Bayley, H. *J. Am. Chem. Soc.* **2012**, *134*, 2781.
(12) Hong, J. *Nanotechnology* **2008**, *19*, 165205.

(13) McNally, B.; Singer, A.; Yu, Z.; Sun, Y.; Weng, Z.; Meller, A. *Nano Lett.* **2010**, *10*, 2237.
(14) Cecchini, M. P.; Wiener, A.; Turek, V. A.; Chon, H.; Lee, S.; Ivanov, A. P.; McComb, D. W.; Choo, J.; Albrecht, T.; Maier, S. A.; Edel, J. B. *Nano Lett.* **2013**, *13*, 4602.
(15) van den Hout, M.; Vilfan, I. D.; Hage, S.; Dekker, N. H. *Nano Lett.* **2010**, *10*, 701.
(16) Ivanov, A. P.; Instuli, E.; McGilvery, C. M.; Baldwin, G.; McComb, D. W.; Albrecht, T.; Edel, J. B. *Nano Lett.* **2011**, *11*, 279.
(17) Tsutsui, M.; Rahong, S.; Iizumi, Y.; Okazaki, T.; Taniguchi, M.; Kawai, T. *Sci. Rep.* 2011, *146*.
(18) Storm, A. J.; Chen, J. H.; Zandbergen, H. W.; Dekker, C. *Phys. Rev. E* **2005**, *71*, 051903.
(19) Chang, H.; Kosari, F.; Andreadakis, G.; Alam, M. A.; Vasmatzis, G.; Bashir, R. *Nano Lett.* **2004**, *4*, 1551.
(20) Schneider, G. g. F.; Kowalczyk, S. W.; Calado, V. E.; Pandraud, G. g.; Zandbergen, H. W.; Vandersypen, L. M. K.; Dekker, C. *Nano Lett.* **2010**, *10*, 3163.
(21) Merchant, C. A.; Healy, K.; Wanunu, M.; Ray, V.; Peterman, N.; Bartel, J.; Fischbein, M. D.; Venta, K.; Luo, Z.; Johnson, A. T. C.; Drndić, M. *Nano Lett.* **2010**, *10*, 2915.
(22) Wanunu, M.; Dadosh, T.; Ray, V.; Jin, J.; McReynolds, L.; Drndic, M. *Nat. Nano* **2010**, *5*, 807.
(23) Wei, R.; Gatterdam, V.; Wieneke, R.; Tampe, R.; Rant, U. *Nat. Nano* **2012**, *7*, 257.
(24) Kowalczyk, S. W.; Kapinos, L.; Blosser, T. R.; Magalhaes, T.; van Nies, P.; LimRoderick, Y. H.; Dekker, C. *Nat. Nano* **2011**, *6*, 433.
(25) Wanunu, M.; Morrison, W.; Rabin, Y.; Grosberg, A. Y.; Meller, A. *Nat. Nano* **2010**, *5*, 160.
(26) Niu, X.; Gielen, F.; Edel, J. B.; deMello, A. J. *Nat. Chem* **2011**, *3*, 437.
(27) Jain, T.; Guerrero, R. J. S.; Aguilar, C. A.; Karnik, R. *Anal. Chem.* **2013**, *85*, 3871.
(28) Kawano, R.; Osaki, T.; Sasaki, H.; Takeuchi, S. *Small* **2010**, *6*, 2100.
(29) Actis, P.; Mak, A.; Pourmand, N. *Bioanal. Rev.* **2010**, *1*, 177.
(30) Morris, C. A.; Friedman, A. K.; Baker, L. A. *Analyst* **2010**, *135*, 2190.
(31) Rodolfa, K. T.; Bruckbauer, A.; Zhou, D.; Korchev, Y. E.; Klenerman, D. *Angew. Chem., Int. Ed.* **2005**, *117*, 7014.
(32) Ying, L.; Bruckbauer, A.; Zhou, D.; Gorelik, J.; Shevchuk, A.; Lab, M.; Korchev, Y.; Klenerman, D. *Phys. Chem. Chem. Phys.* **2005**, *7*, 2859.
(33) Bruckbauer, A.; James, P.; Zhou, D.; Yoon, J. W.; Excell, D.; Korchev, Y.; Jones, R.; Klenerman, D. *Biophys. J.* **2007**, *93*, 3120.
(34) Piper, J. D.; Li, C.; Lo, C.-J.; Berry, R.; Korchev, Y.; Ying, L.; Klenerman, D. *J. Am. Chem. Soc.* **2008**, *130*, 10386.
(35) Karhanek, M.; Kemp, J. T.; Pourmand, N.; Davis, R. W.; Webb, C. D. *Nano Lett.* **2005**, *5*, 403.
(36) Gao, C.; Ding, S.; Tan, Q.; Gu, L.-Q. *Anal. Chem.* **2009**, *81*, 80.
(37) Zhang, B.; Wood, M.; Lee, H. *Anal. Chem.* **2009**, *81*, 5541.
(38) Umehara, S.; Karhanek, M.; Davis, R. W.; Pourmand, N. *Proc. Natl. Acad. Sci. U.S.A.* **2009**, *106*, 4611.
(39) Steinbock, L. J.; Otto, O.; Chimerel, C.; Gornall, J.; Keyser, U. F. *Nano Lett.* **2010**, *10*, 2493.
(40) Wei, C.; Bard, A. J.; Feldberg, S. W. *Anal. Chem.* **1997**, *69*, 4627.
(41) Tabard-Cossa, V.; Trivedi, D.; Wiggin, M.; Jetha, N. N.; Marziali, A. *Nanotechnology* **2007**, *18*, 305505.
(42) Lubensky, D. K.; Nelson, D. R. *Biophys. J.* **1999**, *77*, 1824.
(43) Ling, D.; Ling, X. S. *J. Phys: Condens. Matter* **2013**, *25*, 375102.
(44) Smeets, R. M. M.; Keyser, U. F.; Krapf, D.; Wu, M.-Y.; Dekker, N. H.; Dekker, C. *Nano Lett.* **2006**, *6*, 89.
(45) Chen, P.; Mitsui, T.; Framer, D. B.; Golovchenko, J.; Gordon, R. G.; Branton, D. *Nano Lett.* **2004**, *4*, 1333.
(46) Li, J.; Gershow, M.; Stein, D.; Brandin, E.; Golovchenko, J. A. *Nat. Mater.* **2003**, *2*, 611.
(47) Henrickson, S. E.; Misakian, M.; Robertson, B.; Kasianowicz, J. J. *Phys. Rev. Lett.* **2000**, *85*, 3057.
(48) Zhang, J.; Shklovskii, B. I. *Phys. Rev. E: Stat. Phys., Plasmas, Fluids, Relat. Interdiscip. Top.* **2007**, *75*, 021906.
(49) Meller, A.; Branton, D. *Electrophoresis* **2002**, *23*, 2583.
(50) Wanunu, M.; Sutin, J.; McNally, B.; Chow, A.; Meller, A. *Biophys. J.* **2008**, *95*, 4716.
(51) Fologea, D.; Uplinger, J.; Thomas, B.; McNabb, D. S.; Li, J. *Nano* **2005**, *5*, 1734.
(52) Brewer, L. R.; Bianco, P. R. *Nat. Methods* **2008**, *5*, 517.
(53) Ismagilov, R. F.; Stroock, A. D.; Kenis, P. J. A.; Whitesides, G.; Stone, H. A. *Appl. Phys. Lett.* **2000**, *76*, 2376.